Modeling and Fabrication of Scalable Tactile Sensor Arrays for Flexible Robot Skins

Mohammad Nasser Saadatzi, *Member, IEEE,* Joshua R. Baptist, Zhong Yang, *Student Member, IEEE,* Dan. O. Popa, *Senior Member, IEEE*

***Abstract*— Artificial robot skins capable of multi-modal tactile feedback are anticipated to revolutionize how robots perceive their immediate surroundings and how they collaborate with humans on tasks more complicated and dynamic than currently possible. Efforts to develop tactile skins must tackle significant hurdles related to flexibility, robustness, and scalability of sensors. In this paper, a flexible tactile sensor array is developed to address these hurdles via a novel sensor geometry and thermal compensation technique. This tactile skin relies on a polymeric piezoresistive array of strain gauges with a novel star-shaped geometry. Due to their radial symmetry, the proposed strain gauges exhibit a biaxial response to local strain-stress loading, avoiding "blind spots" in the vicinity of individual tactels. The sensors are fabricated using gold electrodes and piezoresistive polymers (PEDOT:PSS) micro-patterned on a flexible polyimide substrate enclosed in a compliant silicone matrix. The sensor is first modeled using multiphysics finite elements software to guide design choices for a variety of geometric parameters under various load profiles and locations with respect to the gauge's center. A novel homogeneous thermal compensation technique is proposed which packages the sensors on the opposite sides of a flexible carrier. This thermal compensation technique achieves a 10-fold attenuation in temperature drifts, as well as a double sensitivity in term of strain measurement. After numerical modeling, a 4x4 tactile array with the optimal geometry obtained through simulation was fabricated and interfaced to a custom-made electronic data acquisition system. Samples were tested using an automated dynamic force experimental testbed. The tactile skin array was experimentally characterized in terms of force sensitivity, spatial response, dynamic bandwidth, and temperature drift. The array exhibits sensitivity of 1125 nV/N in the range of 0-0.5 N, sensitivity of 412 nV/N in the range of 0.5-2.3 N, hysteresis of 11.13%, dynamic bandwidth of 1.49 Hz, and temperature sensitivity of 6 nV/°C, averaged among individual sensors.**

***Index Terms*—Artificial robot skin, tactile sensing, strain gauge, piezoresistive, thermal compensation, PEDOT:PSS, multiphysics finite-element analysis, microfabrication, physical human-robot interaction.**

I. Introduction

HUMANS depend on the sense of touch to feel tactile stimuli around them and to perceive their immediate environment. The sense of touch complements the sense of sight by collecting data unobtainable through vision such as surface roughness and temperature. Therefore, the mimicry of tactile sensing capability in humans has held great interest among researchers in the field of robotics, for applications in human-robot interaction and healthcare delivery [1-10]. As robots proliferate in household and industrial environments, an artificial skin capable of providing human-like tactile sensory perception can facilitate their safe and autonomous operation in increasingly closer proximity with humans [11].

Scientific literature spanning the last 3 decades depicts various endeavors of endowing robotic systems with tactile sensing capability [12] using various sensing technologies [13, 14]. For instance, Lumelsky and colleagues developed a multi-modal artificial skin for a robotic manipulator using a covering of infra-red sensing elements to facilitate physical human-robot interaction (pHRI) [15]. Mittendorfer and Cheng covered a HEP-2 robot as well as a KUKA manipulator with a modular electronic skin capable of sensing tactile variables such as force and temperature, as well as proximity and acceleration [16]. Schmitz and colleagues installed artificial skin patches, with distributed capacitive pressure sensing capability, on a variety of humanoid robots to endow them with tactile sensing ability [17]. Lepora and colleagues placed pressure-sensitive tactile units on an iCub's palm and studied various tactile and position resolutions by overlapping the sensing elements [18]. Mukai and colleagues utilized piezoresistive semi-conductor pressure sensing elements placed on various body locations of a humanoid robot to provide tactile feedback during complicated tasks such as lifting a human with the robot's arms [19]. Asfour and colleagues equipped a humanoid robot with force-sensitive pads, mounted on its shoulders and arms, to enable tactile perception and human-robot interaction [20]. Iwata and Sugano covered a humanoid robot's hands, arms, and trunk with distributed force sensing units and achieved large-area tactile sensing [21]. Cannata and colleagues introduced a network of modular tactile skin units with force-sensing capability based on capacitive transduction technology, and deployed it on a humanoid robot's upper arm [22]. Yet, despite enormous progress in the fabrication and utilization of robot skins [5, 10, 12, 15-27], the current tactile sensing technology continues to face limitations related to reliability and scalability. For comprehensive reviews of the extant literature in this domain, refer to [15, 28-31].

A multitude of technologies have been used to develop tactile feedback systems [13, 14]. However, recent efforts have been mainly concentrated on silicon-based sensors [31-38]. Silicon

This study was supported by National Science Foundation grants no. IIS-1208623, IIP-1534124, and IIP-1713741.

Authors are with Next Generation Systems Group, Department of Electrical and Computer Engineering, University of Louisville, Louisville, KY, 40292 USA. (e-mail: mn.saadatzi, joshua.baptist, zhong.yang, dan.popa) @louisville.edu

demonstrates large piezoresistive coefficients [39] and is supported by well-developed processing technologies, rendering it an attractive choice of material. Silicon-based sensors are, in general, constructed on wafers and then diced and incorporated within tiny modules along with microelectronic integrated circuits. Such processing technique, however, does not easily lend itself to applications where large-area tactile monitoring is required. Furthermore, tactile sensing requires that the sensor network be flexibly installed in intimate contact with non-planar surfaces of robots in order to avoid "blind spots." Brittle and rigid nature of silicon-based sensors is incompatible with this requirement and limits its application as a substrate of continuously flexible artificial skins. Although silicon can be made more flexible through complicated, costly processes, such as reducing its thickness [31], comes at the cost of decreasing robustness to physical impacts. This is a serious drawback as tactile sensors function through physical contact with the environment. Flexible sensor arrays capable of covering a large non-planar area can afford transformational opportunities for tactile sensing technology. One approach to develop such artificial skins is to fabricate a distributed array of individual tactile sensors (e.g., strain gauges) incorporated on a flexible substrate, enabling measurement of contact location and load [14]. For example, Kim and colleagues created a flexible array of strain gauges each of which capable of measuring normal forces ranging from 0-1 N [40]. Similarly, Choi utilized micromachining technology to fabricate a distributed array of strain gauges on a flexible film that enabled placement of the sensor array on a curved surface [41]. The sensors demonstrated a force measurement capability in the range of 0-0.8 N.

Most tactile sensors suffer from inherent temperature-induced drifts which negatively influence the repeatability of measurements [28]. Therefore, a major challenge is to deconvolute pressure-induced signals from temperature drifts. A number of research groups have addressed this challenge via heterogeneous integration of pressure- and temperature-sensing elements in order to compensate for temperature contributions to the sensors' outputs [24, 42]. For instance, Yang and colleagues used a discrete temperature sensor chip per tactile sensor, on the back of the flexible substrate, so as to discriminate between temperature and force outputs [43]. Graz and colleagues developed a large-area artificial skin with tactile cells each of which including a temperature sensor and a pressure sensor side by side, and differentiated the outputs under simultaneous stimulations [44]. This approach, although effective, requires a large number of temperature sensing elements and a dedicated scanning and data collection circuitry. Furthermore, design and fabrication of the additional temperature sensors on the same substrate as well as their calibration and data processing bring about challenges in terms of spatial density, wiring interconnects, computational intensity, and, hence, scaling. In this study, a novel and effective thermal compensation technique is proposed by homogeneous integration of strain sensing elements with opposing sensitivity to strain and identical sensitivity to thermal stimulus. The proposed technique, as explained in detail in section III, achieves a 10-fold reduction in temperature sensitivity over a 50 °C temperature range, and also affords a double sensitivity in term of strain measurement.

Strain gauges are sensing elements that are used to measure strain at a single point on a surface, and produce variations in their electrical properties, such as resistance or capacitance. These variations are then correlated to the experienced strain by a coefficient known as the gauge factor [45]. A single strain gauge is capable of sensing strain effectively along a single direction at a given point. This uni-directional functionality necessitates the usage of multiple strain gauges to measure strain on a two-dimensional plane at the same point. To precisely evaluate loads that act in a biaxial strain state at a given point on the surface, a number of strain gauges are positioned in certain geometrical configurations, such as rectangular and triangular strain gauge rosettes [46]. In the context of artificial electronic skins based on strain gauge architecture, Engel and colleagues implemented an array of strain gauges in a lattice format in order to measure strains along both horizontal and vertical axes [42]. Yang and colleagues used an array of tactile elements each of which containing multiple strain gauges in a rosette arrangement in order to monitor strain across a surface [47]. In this paper, we propose a novel star-shaped strain gauge which demonstrates a symmetric biaxial response thanks to its radial symmetry, and hence, does not experience "blind spots" in its vicinity. Such biaxial sensitivity obviates the necessity of using multiple strain gauges at each point, immensely facilitating the scalability of large-area, spatially-dense tactile arrays.

We extend the single gauge design to an artificial robot skin prototype consisting of a 4x4 array of homogeneously temperature-compensated, piezoresistive strain gauges. The gauges were composed of a gold micro-patterned star-shaped structure and an organic piezoresistive layer fabricated on a continuous, flexible polyimide thin film. The array of strain gauges were subsequently encapsulated inside a flexible polymer matrix, and interfaced with a custom-made electronic data acquisition system. The piezoresistive material used in these sensors was Poly(3,4-ethylenedioxythiophene)-poly(styrenesulfonate), or PEDOT:PSS in short, which is a flexible, organic piezoresistive polymer [48]. In this paper, we patterned PEDOT:PSS on the sensor array via a novel wet lift-off photolithographic technique which allows batch fabrication of the tactile arrays, facilitating scalability of production. Prior to fabrication, a parametric finite-element analysis (FEA) of the sensors was performed in the COMSOL® Multiphysics software in order to find the optimal sensor geometry. In the numerical analyses, varying forces and application locations with respect to the sensor's center were simulated. Ultimately, automated characterization procedures were performed to evaluate the sensors' behavior in terms of dynamic force-to-strain characteristics, temperature sensitivity, spatial sensitivity, and dynamic bandwidth.

The experimental data demonstrated a close agreement with the simulation trends obtained from FE modeling in terms of biaxial sensitivity and circular symmetry. According to the empirical data collected in the range of 0-50 °C, the proposed thermal compensation technique attenuated the drifts caused by temperature variations to 10% of the drifts when no compensation was employed. The sensor array exhibits a repeatable behavior in the range of 0-2.3 N with a sensitivity of 1125 nV/N in the range of 0-0.5 N, sensitivity of 412 nV/N in the range of 0.5-2.3 N, hysteresis of 11.13%, dynamic

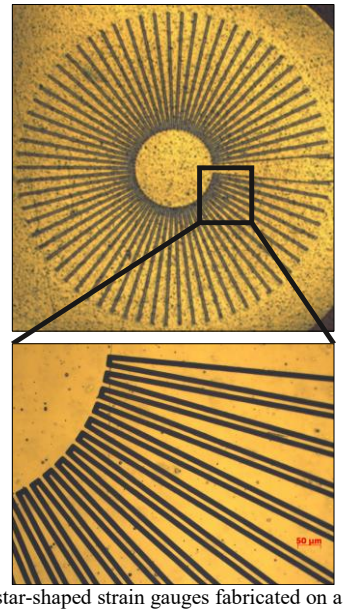

Fig. 1. Proposed star-shaped strain gauges fabricated on a flexible polyimide substrate (top), and magnified radial spokes (bottom).

bandwidth of 1.49 Hz, and temperature sensitivity of 6 nV/°C, averaged among individual sensors. These performance metrics make the developed robot skin suitable to future pHRI applications where humans push and pull to guide robots using programming by demonstration.

The remainder of this paper is organized as follows. Section II presents the proposed strain gauge structure and numerical modelling. Section III describes the procedure for the fabrication of sensor array, PEDOT:PSS formulation, thermal compensation, and packaging. The data acquisition system and experimental setup are outlined in section IV. Section V presents the characterization and experimental results, and, finally, section VI discusses the results and concludes the paper.

II. Tactel Design and Modeling

The tactel sensor proposed in this study is based on a star-shaped strain gauge that is micro-fabricated on a flexible polyimide film (i.e., Kapton), a thin piezoresistive layer atop (i.e., PEDOT:PSS), and a protective layer covering the array (Fig. 1). The piezoresistive layer and the gold structure form a conductive medium with a variable electrical resistance which is a function of surface deformations caused by external load.

To simulate the proposed sensor, a 3-D CAD model of the star-shaped structure was first imported into the COMSOL® simulation environment and put on top of a Kapton layer. Next, a PEDOT:PSS layer was added uniformly on top and in between the gold electrodes. Finally, a Kapton covering was defined on top of the piezoresistive material which in reality protects the sensor from environmental effects such as humidity. Layers of the proposed strain gauge structure are depicted in Fig. 2.

Fig. 2. Various layers of the proposed star-shaped strain gauge

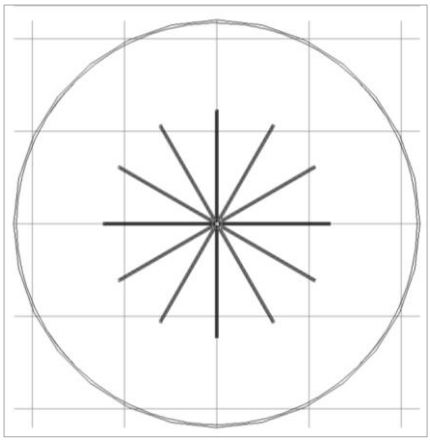

Fig. 3. FEA simulation environment with a simplified sensor structure.

In order to reduce simulation time and avoid convergence issues, simplified models of the sensor structure with only 4, 6, and 12 spokes were analyzed in COMSOL®. Fig. 3 depicts the simplified model with 12 spokes. Other geometric parameters of the sensor (e.g., spokes' length, spokes' width, and spacing between polarities) were kept realistic. Material properties of the artificial robot skin components, and the model's dimensions are specified in Tables I and II, respectively. Furthermore, PEDOT:PSS was simulated by modification of a p-doped silicon piezoresistive material with a longitudinal piezoresistive coefficient of -0.511 nPa^{-1}, transversal piezoresistive coefficient of 0.345 nPa^{-1}, and density of 1011 kg/m^3 [49]. Ultimately, the sensor was placed on a soft membrane which allows for sensor deformation when external load is applied.

TABLE I
Material Properties of Artificial Skin Components

Material	Young's Modulus [GPa]	Poisson's Ratio	Density [kg/m^3]
Gold	70	0.44	19300
Polyimide	2.5	0.34	1420
Membrane	0. 0015	0.47	1100

TABLE II
Simulation Model's Dimensions

Component	Length [mm]	Width [mm]	Height [μm]
Gold structure	4.34	4.34	1
Polyimide	2000	2000	100
Membrane	2000	2000	4000
PEDOT:PSS	1.8	1.4	1
Indenter	4.34	4.34	-

In order to understand the relation between the number of spokes and the gauge's sensitivity, varying forces in the range of 0-5 N were applied on top of the sensors with 4, 6, and 12 spokes. A typical displacement graph of the skin surface is depicted in Fig. 4. Percent changes in the electrical resistance of the strain gauges are shown in Fig. 5. According to this figure, higher numbers of spokes lead to sensors with larger sensitivities. The actual sensor, hence, was fabricated with the largest number of spokes (i.e., 67) allowed by the spatial density of the tactel and sensor array (Fig. 1).

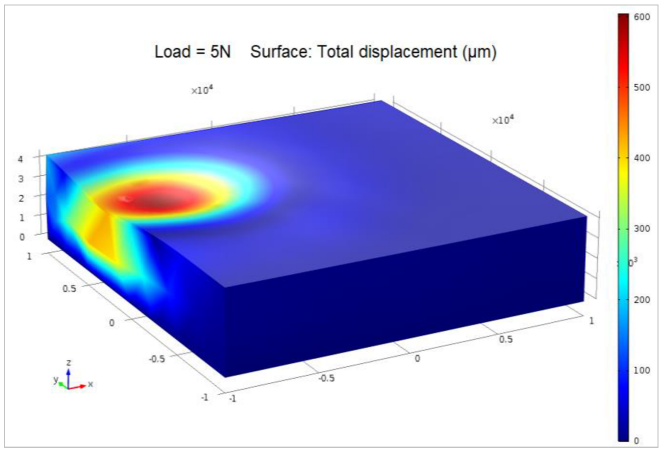

Fig. 4. Surface deformation due to normal load application along the z-axis.

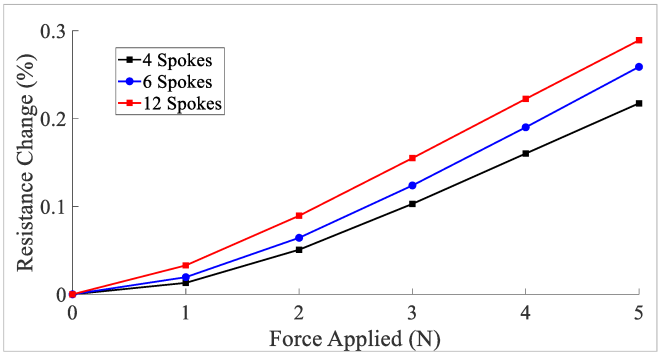

Fig. 5. Changes in electrical resistance due to load application on sensors with different number of spokes.

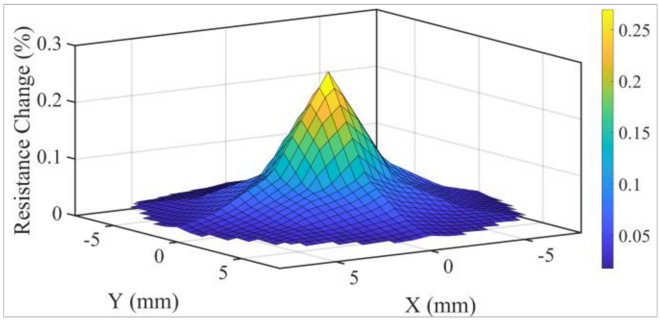

Fig. 6. Sensor's spatial response to load application at various locations in its vicinity.

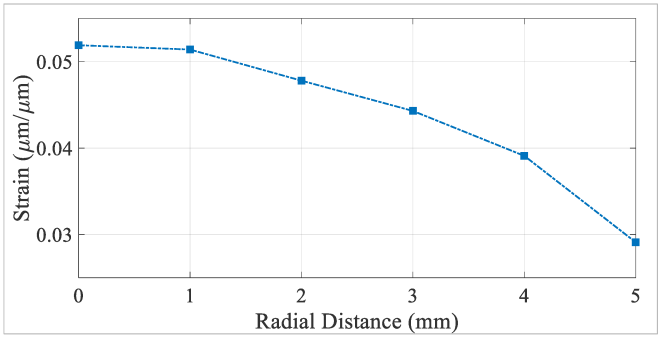

Fig. 7. Strain distribution on the skin surface as a function of radial distance.

Additionally, to inspect the spatial sensitivity of the proposed structure, application of forces (with amplitude of 5 N) on different spots in the vicinity of the sensor was simulated. Fig. 6 depicts these resistance variations for different loading locations. As can be seen, the sensor's behavior in its vicinity is radially symmetric, showing identical, biaxial responses to load applied along X and Y axes. According to this figure, the sensor's response is largest when force is applied on its center, and is a function of the distance between the load location and the sensor's center. Similarly, Fig. 7 depicts the strain on the skin surface, caused by the local load applications, as a function of distance from the sensor's center. Due to the radial geometry of the sensors and the multi-axial strain distribution on the sensor structure, von Mises equivalent strain was utilized. Von Mises strain takes into account the mean value of all strain components as the following:

$$\varepsilon_{eq} = \frac{1}{\sqrt{2}(1+\nu)}\left[(\varepsilon_x - \varepsilon_y)^2 + (\varepsilon_y - \varepsilon_z)^2 + (\varepsilon_z - \varepsilon_x)^2 + \frac{3}{2}(\gamma_{xy}^2 + \gamma_{yz}^2 + \gamma_{xz}^2)\right]^{1/2} \quad (1)$$

where ε and γ are the appropriate strain components in each direction, and ν is the effective Poisson's ratio. According to Fig. 7, von Mises strain displays a decaying trend with increasing radial distance from the sensor's center point toward the boundaries.

TABLE III
MATERIAL PROPERTIES OF ARTIFICIAL SKIN COMPONENTS

Length [mm]	Width [μm]	Spacing [μm]	Resistance Variation [%]
1.0	10	10	0.2959
1.0	10	20	0.2992
1.0	20	10	0.3412
1.0	20	20	0.2793
1.2	10	10	0.3549
1.2	10	20	0.3014
1.2	20	10	0.3511
1.2	20	20	0.2845

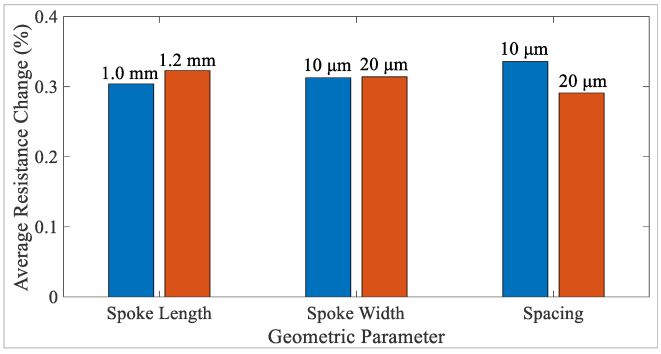

Fig. 8. Average resistance change for each geometric parameter.

In this study, a simulation experiment with a factorial design was also performed in order to understand how geometric parameters of the strain gauge affect its sensitivity. To that end, a number of geometrical parameters of the sensor structure, including spokes' length and width, as well as the spacing between the polarities, were simulated in COMSOL®. The studied levels for width, length, and spacing factors were {10 μm, 20 μm}, {1 mm, 1.2 mm}, and {10 μm, 20 μm}, respectively. The results are summarized in Table III, and the average resistance change for each geometry parameter is depicted in Fig. 8. Table III and Fig. 8 suggest that longer spokes and narrower spacing tend to bring about larger sensitivities on average, whereas the effect of spoke's width on

the gauge's sensitivity on average is negligible. The effect of spoke width, however, is not uniform across other factors. For instance, for constant spoke length of 1.0 mm and spacing of 10 µm, the relative change for the two levels of spoke width is high (i.e., 0.2959% vs. 0.3412%). Hence, the effect of width depends on level of other factors, and, as such, must be carefully studied case by case.

The obtained optimal values were used to fabricate strain gauge arrays in the following section. In addition, although having different sensitivities, all geometric specifications result in strain gauges with similar biaxial trends in their Gaussian-shaped response illustrated in Fig. 6. In general, the existence of blind spots depends on the spatial sensitivity of individual sensors and the array density, as well as the amplitude of applied load. According to the radial spatial sensitivity of fabricated gauges (due to the star-shaped geometry), gauges were organized in a 4x4 matrix layout with a lateral center-to-center distance of 10.0 mm (Fig. 9). In this scenario, with the overlapping sensitivity of such spatially-dense sensor matrix, the skin array avoids blind spots for applied forces as small as 150 mN on any location of the skin surface. Forces with smaller amplitudes may remain undetected if applied far away from sensors' center points.

III. Fabrication of Tactile Skin Array

A. Fabrication of electrodes

The strain gauge sensors proposed in this paper were implemented by fabricating piezoresistive microstructures on a polyimide substrate (Kapton with 50 µm thickness) through photolithographic techniques. At first, a Kapton sheet with an appropriate size was obtained and cleaned with solvent (i.e., Acetone and Isopropyl alcohol) and adhered to a carrier wafer coated with photoresist (i.e., MicroChem SPR-220-3.0) using a brayer and cleanroom wipe while at a temperature of 90 ºC. The Kapton surface was then exposed to O_2 plasma (Technics RIE - 300mT, 30 SCCM, 75 Watts RF, 45 Seconds) to remove any contaminants and particles. Next, to pattern the electrodes and traces, the wafer was covered with a bi-layer resist (MicroChem LOR 10-B and SPR-220-3.0), hard-baked at 115 ºC for one minute, and transferred to a mask aligner where it was exposed for 11 seconds. Upon exposure, the stack underwent another baking step at 115 ºC for one minute and was cleaned through reactive ion etching (RIE) process with the previously mentioned recipe. Next, 300 nm thick gold was directly deposited on the patterned substrate using a conventional sputter deposition system. Such direct deposition of gold with DC sputtering produced great adhesion to the polyimide substrate without any cracks. The stack was then placed into a sonicated lift-off bath of Acetone for at least 15 minutes to reveal the sensor features and dissolve the resist interface holding the freshly patterned Kapton sheet to the Si carrier wafer. Subsequently, the Kapton was removed from the wafer and rinsed with solvent before further processing. The substrate with the gold star-shaped structure was then laminated onto a new wafer through identical aforementioned steps and cleaned with O_2 RIE. Next, the stack was coated with a thin layer of resist, followed by hard-baking, exposure in a mask aligner,

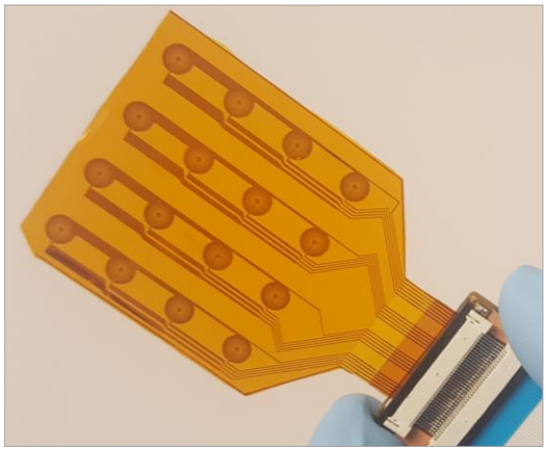

Fig. 9. 4x4 sensor array with signal routing and interconnection patterned as Zero-Insertion Force (ZIF) contact pads.

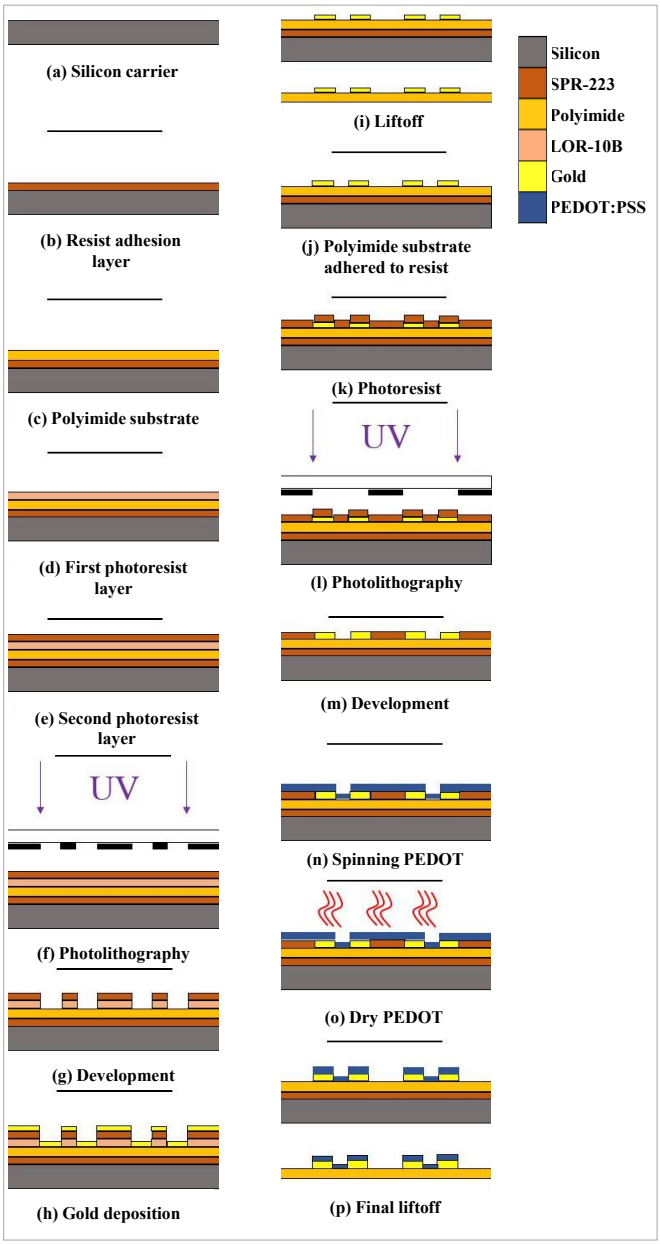

Fig. 10. Microfabrication process including patterning gold structures on polyimide substrate followed by depositing PEDOT:PSS.

post-exposure-baking, and cleaning in an RIE process. The microfabrication process is outlined in Fig. 10.

B. Development and deposition of PEDOT:PSS

The choice of material as a base for our pressure-sensing array in this study was PEDOT:PSS obtained from Sigma-Aldrich, USA, which is an organic piezoresistive material with high gauge factor and flexible nature [48]. In this study, we employed a spin-coating depositing method and wet lift-off to pattern PEDOT:PSS on the strain gauge structures, which enables cost-effective, batch processing of large-area arrays, promoting manufacturing scalability. Alternatively, this material can also be 3D printed, but current dispensing technologies, especially at comparable costs in volume production, face challenges in printing resolution, layer thickness, and deposition uniformity [50, 51]. Furthermore, ink development for inkjet/jetting applications is in general more complex and have more factors to consider [52-54]. Ink-jettable and other regular forms of PEDOT:PSS obtained from commercial chemical manufacturers cannot be used directly for the spinning process and, hence, must undergo a pre-conditioning step to fit this deposition method by increasing its wettability. Therefore, in order to uniformly spin-coat PEDOT:PSS on the substrate and gold structures, we prepared a colloid of %0.8 PEDOT:PSS with Methanol solvent in a one-to-one volume ratio. This ratio was selected as it provided a desirable viscosity, low surface tension, and uniform coating. The colloid was sonicated for 15 minutes to obtain a consistent mixture. Upon sonication, the wafer was spin-coated with the PEDOT:PSS mixture at 2000 rpm for 45 seconds only on openings over the star-shaped structures, and then left to dry in a vacuum oven. Following this step, the stack underwent a wet lift-off process in an Acetone bath to remove the resist and leave the piezoresistive pattern exactly over the star-shaped structures. PEDOT:PSS exhibited extremely well adhesion to polyimide. As such, there was no concern about it lifting-off from the substrate during wet processing. The thickness of the PEDOT:PSS film was 135 nm on average as measured by an atomic force microscope (Asylum Research MF3D). Finally, the substrate was transferred to a convection oven to remove excess moisture and was sealed with a Kapton tape covering to avoid moisture permeation and contaminant adsorption. This was accomplished simply by hand lamination and treatment in vacuum. Finally, sensor arrays were manually diced for subsequent use. Total completed thickness of sensors was 125 microns.

C. Lamination of sensors for thermal compensation

Temperature drift of sensors in the context of artificial electronic skin has been traditionally addressed via heterogeneous integration of temperature sensing elements with tactile sensors [24, 42-44]. In the current study, a novel thermal compensation technique is proposed via homogeneous integration of merely force-sensing elements (i.e., strain gauges). In this technique, two identical sensor arrays were pasted back to back such that every strain gauge was paired with an identical sensor exactly on the other side. Different layers of such double-sided sensor pair is illustrated in Fig. 11.

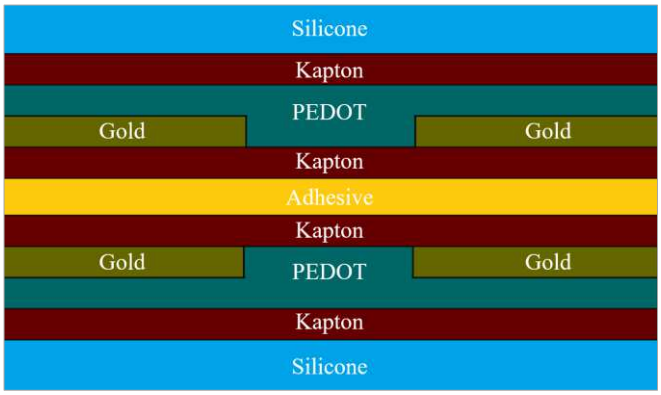

Fig. 11. Various layers of temperature-compensated tactel encapsulated within a silicone membrane.

To sense the strain exerted on the sensor pair, the two sensors were arranged as a Wheatstone half bridge as depicted in Fig. 12. Since the sensors are laminated on the opposite side of each other, in a back-to-back configuration, they experience opposing strains (i.e., compression vs. tension) when load is applied on the pair (Fig. 12). On the other hand, because both are located at the same spot, they experience identical ambient temperature and, thus, identical thermal responses (i.e., electrical resistance variation) are induced. In Fig. 12, R_1 and R_2 are the resistance of the paired strain gauges, V_E is the excitation voltage, and V_O is the output voltage of the half bridge. Since R_1 and R_2 are functions of both strain, ε, and temperature, T, the output voltage can be formulated as

$$V_O = \frac{R_1(\varepsilon,T)\,V_E}{R_1(\varepsilon,T)+R_2(\varepsilon,T)} \tag{2}$$

Variations in the output voltage caused by thermal stimuli is

$$\frac{dV_O}{dT} = \frac{\partial V_O}{\partial R_1}\frac{dR_1}{dT} + \frac{\partial V_O}{\partial R_2}\frac{dR_2}{dT} \tag{3}$$

$$\frac{dV_O}{dT} = \frac{R_2\,V_E}{(R_1+R_2)^2}\frac{dR_1}{dT} - \frac{R_1\,V_E}{(R_1+R_2)^2}\frac{dR_2}{dT} \tag{4}$$

$$\frac{dV_O}{dT} = \frac{V_E}{(R_1+R_2)^2}\left(R_2\frac{dR_1}{dT} - R_1\frac{dR_2}{dT}\right) \tag{5}$$

As temperature fluctuations produce similar responses in both sensors, and the sensors' resistances at rest are theoretically identical, the second term in (5) approaches zero, rendering V_O invariable to thermal effects. Similarly, variations in the output voltage due to strain is:

$$\frac{dV_O}{d\varepsilon} = \frac{\partial V_O}{\partial R_1}\frac{dR_1}{d\varepsilon} + \frac{\partial V_O}{\partial R_2}\frac{dR_2}{d\varepsilon} \tag{6}$$

$$\frac{dV_O}{d\varepsilon} = \frac{R_2\,V_E}{(R_1+R_2)^2}\frac{dR_1}{d\varepsilon} - \frac{R_1\,V_E}{(R_1+R_2)^2}\frac{dR_2}{d\varepsilon} \tag{7}$$

$$\frac{dV_O}{d\varepsilon} = \frac{V_E}{(R_1+R_2)^2}\left(R_2\frac{dR_1}{d\varepsilon} - R_1\frac{dR_2}{d\varepsilon}\right) \tag{8}$$

Since the sensors' responses caused by pressure applied on top of the sensor pair demonstrate opposing directions (i.e., one's electrical resistance increases while the other one decreases), the second term in (8) is twice as large as compared to a single sensor's response, producing a double sensitivity to local geometric deformations.

$$\frac{dV_O}{d\varepsilon} \simeq \frac{V_E}{R_1+R_2}\frac{dR_1}{d\varepsilon} \tag{9}$$

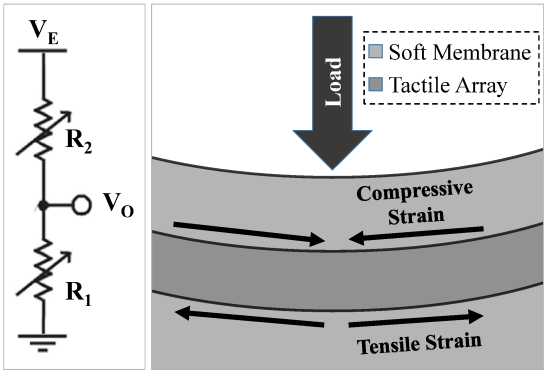

Fig. 12. Paired strain gauges electrically configured as a Wheatstone half bridge (left), and tactile array experiencing local load (right).

D. Wiring and interconnection

In the design and fabrication of the proposed artificial robot skin, we paid special attention to quick and reliable connection of the sensor array to external electronics for signal conditioning and data acquisition, as the utility of such large-area, distributed network of sensors becomes quickly limited by the wiring interconnects, hampering scalability. Traditional electrical wires and bonding are bulky as compared to components of the sensor array, and would not provide a durable interface with flexible material inside the skin. To address this challenge, conductive paths were fabricated on the same carrier in-plane with the star-shaped structures during the microfabrication process. The conductive paths were routed to the edge of the substrate to produce an electrical terminal fashioned as a zero insertion-force (ZIF) connector pinout, as shown in Fig. 9. Since, the sensor array was double-sided (i.e., laminated back to back for the purpose of thermal compensation), there were traces on both sides of the array. Hence, in order to allow electrical connection to traces on both sides, pluggable ZIF connector sockets with dual-contact style were utilized.

E. Encapsulation

The fabricated sensor array was encapsulated within an elastic matrix in order to provide collision absorption and mechanical compliance. More importantly, such continuously deformable membrane functions as a pressure diffusion layer allowing local geometrical deformations of the strain gauges due to load application. In this study, a multi-step casting process was utilized to mold silicone polymer all around the sensor array. Our choice of elastomer material was RTV silicone rubber (Dow Corning 4250-S polymer) due to its chemical inertness, high elongation capability, and ease of casting. For the sake of casting, a two-part mold (i.e., a base mold and a completion mold holder) was CAD modeled and 3-D printed. The two parts were first sprayed with a release agent (i.e., Parylene) in order to avoid chemical reaction between the 3-D printing material (i.e., resin) and the elastomer. Subsequently, the base mold was utilized to cast a base membrane, followed by placement of the sensor array atop. Next, the completion mold holder was mounted and filled with the RTV rubber mixture. The stack was then transferred to a heat-accelerated degasification vacuum in order to remove bubbles and cure the membrane. A typical casting procedure to encapsulate our sensor arrays inside a 5-mm thick silicone matrix is shown in Fig. 13. For more information refer to our previous work in [55].

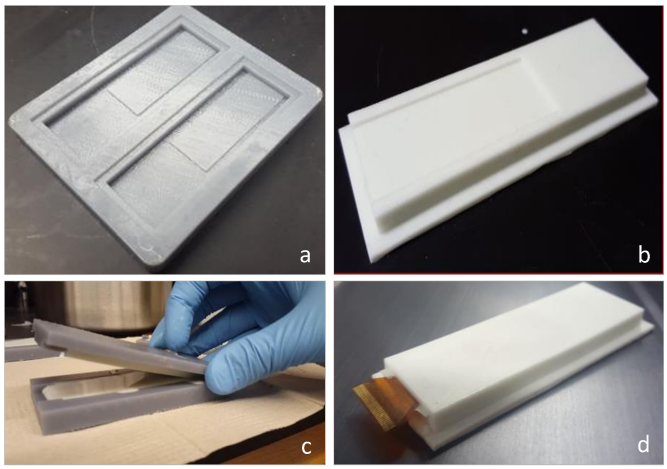

Fig. 13. Encapsulation procedure: (a) 3-D printed base mold, (b) base membrane casted using the base mold, (c) 3-D printed completion mold encompassing the base membrane and the sensor array, and (d) the final over-molded sensor array as a robot skin patch.

IV. Experimental Testing and Characterization

A. Electronic data acquisition system

In order to measure the sensor array's output signals, a custom-made data acquisition (DAQ) board was developed in house and interfaced with the array. This DAQ contains a signal conditioning stage, instrumentation amplifier, and bi-polar voltage regulation circuitry. To collect data, the DAQ was interfaced with an evaluation module for Texas Instruments ADS1258 chip which is a precision, 16-channel, 24-bit analog-to-digital converter (ADC). The electronic data acquisition system and its block diagram are shown in Fig. 14. In order to address scalability challenges, this DAQ utilizes an innovative software-based calibration scheme without the conventional Wheatstone full bridge per tactel. The on-board ADC features a multiplexer which sequentially switches among the sensors and connects individual Wheatstone half bridges to an external signal conditioning stage designed to remove the DC offset and to perform analog low-pass filtration. The output of this stage is routed to a precision amplification stage, and is subsequently fed back to the ADC. ADS1258 then samples the signal, performs digital filtration, and outputs a stream of data via SPI communication. The evaluation module captures the collected data and transmits them to a computer via a USB port for online data visualization and processing. For more information refer to our previous work in [56, 57]. A custom-made graphical user interface (GUI) was programmed which allows the user to select the tactels of interest as well as the desired sampling frequency. Using the high-resolution data stream provided by the ADC, this GUI implements a software-based calibration scheme at the beginning of each data collection cycle, obviating the need for a separate calibration stage for each individual tactel.

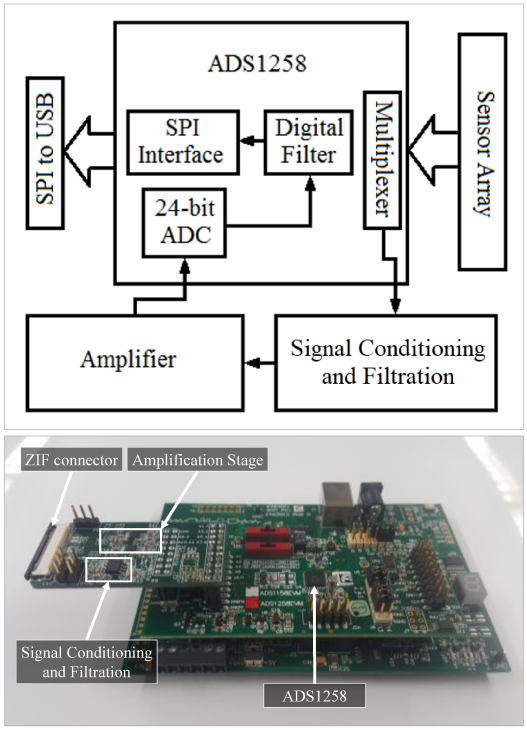

Fig. 14. Block diagram (top) and electronic circuitry (bottom) of data acquisition system.

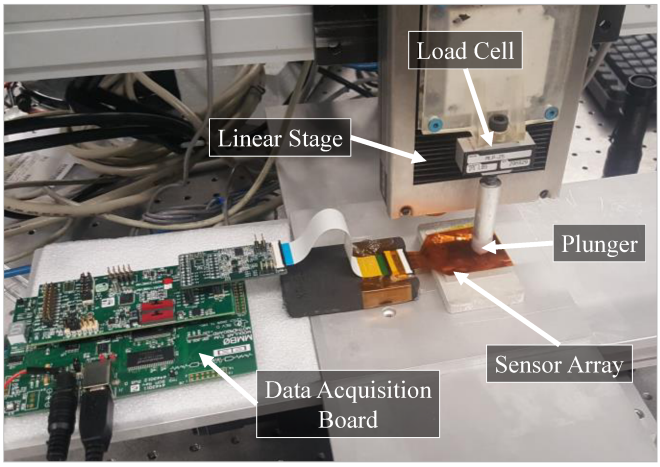

Fig. 15. Experimental setup to automatically apply controlled loads at desired locations on the surface of the artificial skin.

B. *Experimental setup*

Sensor arrays were tested and systematically characterized via an automated experimental setup developed in-house, shown in Fig. 15. This setup involves three perpendicular linear stages, a load cell (to collect reference data), and a real-time controller from National Instruments (cRIO 9074). The skin package is fixated on a mount plate displaced in the X-Y plane using two of the linear stages, while the third stage applies desired load profiles along the Z-axis on different locations of the skin surface using an indenter. To automate the characterization procedure for the whole array, a LabVIEW front panel was programmed and uploaded on the controller, which synchronizes motion of the stages while collecting time-sensitive data from the load cell and the data acquisition system. In this program, using the load cell's output, a real-time proportional-integral-derivative controller was implemented to apply desired force trajectories. The collected data streams from the load cell and the skin array are utilized to study the arrays behavior under static and dynamic loads and characterize the sensors.

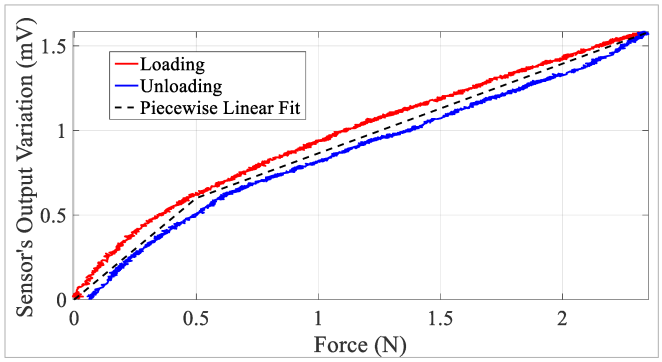

Fig. 16. Typical sensor's characteristic curve, indicating a modest hysteresis.

V. Experimental Results and Discussion

A. *Characteristic curve*

An artificial electronic skin prototype was systematically characterized. For this purpose, a monotonically varying force in the range of 0-2.3 N was exerted on top of each sensor, while the data stream from the DAQ and the readings from the load cell were collected simultaneously. Fig. 16 illustrates a typical characterization curve obtained by establishing the relationship between applied force and sensor's output during a load–unload cycle. According to this figure, the sensor has a hysteresis characteristic curve which is due to the time- and history-dependent viscoelastic nature of the soft silicone membrane. The results show that, for equal loads, the sensor has a larger response during loading than unloading. Quantitatively, a maximum variation of 11.13% was observed in the hysteresis curve. Beyond 2.3 N, more substantial nonlinearity and sensor degradation begin to appear.

According to Fig. 16, two regions can be observed: (a) a linear response below 0.5 N, and (b) an incrementally-linear response beyond 0.5 N. The characteristic curve of each sensor was approximated with a piecewise linear function, representing these two regions. In the range of 0-0.5 N, the results show an average 1125 nV/N sensitivity to applied forces on top of each tactel, and 518 nV/N standard deviation. In the range of 0.5-2.3 N, the average sensitivity and standard deviation are 412 nV/N and 202 nV/N, respectively. This significant variation may be explained by the yield of our microfabrication process, including wet lithography, and molding. Fig. 17 depicts the array's sensitivity in the interval of 0-0.5 N (i.e., slope of the fit) across individual sensors. Furthermore, in order to understand sensitivity changes over time, cyclic stability was evaluated by repeated (n = 5) application of force (F = 1 N) atop a tactile sensor while monitoring the change in its output voltage. To be consistent across iterations, the indenter was held off the skin surface for 5 minutes before loading in order to cancel out hysteresis and memory effects. Under these conditions, the mean and standard deviation of the sensor's output were 971.9 nV and 32.8 nV,

respectively, suggesting a fairly repeatable and stable operation of individual sensors under repetitive exposure to mechanical deformation.

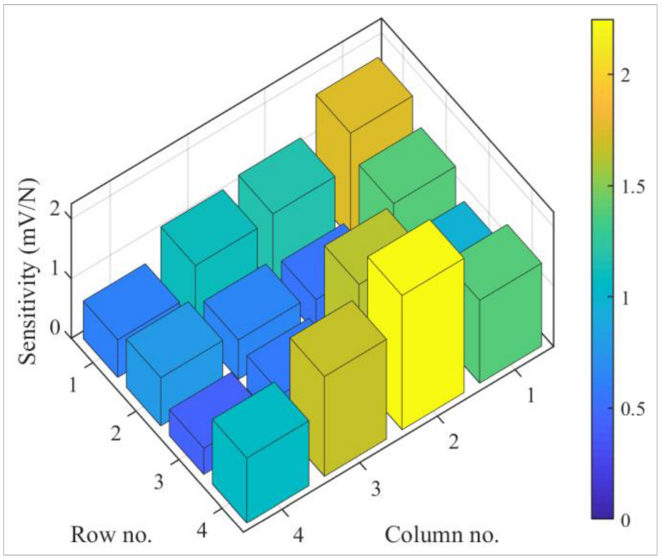

Fig. 17. Individual sensors' sensitivity to force applied atop sensor's center in the range of 0-0.5 N.

B. *Biaxial response*

To test the spatial sensitivity, loads with the amplitude of 2 N were applied on different locations of the skin surface with increasing distances with respect to a sensor's center in both X and Y directions. To be consistent in loading experiments across different locations, the indenter was held off the skin surface for 5 minutes before loading in order to completely cancel out hysteresis and memory effects. Fig. 18 depicts the typical spatial response for each sensor in the skin array. According to this figure, the sensors show similar behavior in both directions, verifying the biaxial response demonstrated by finite-element simulations. Sensors' largest response occurs at their center point while their sensitivity shows a downtrend pattern as the location of applied load moves further away.

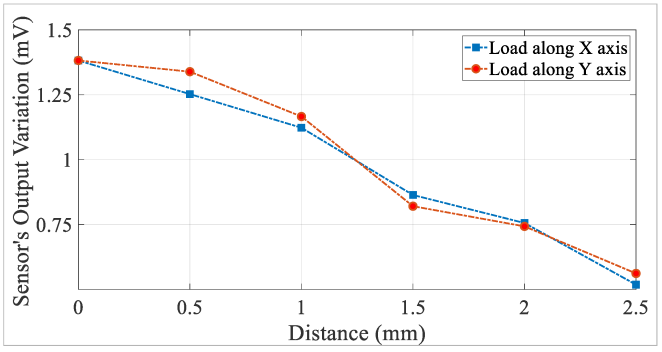

Fig. 18. Typical sensor's spatial sensitivity along X and Y axes.

C. *Bandwidth*

Sensors' bandwidth was calculated by applying a unit step force atop their center point, and measuring the rise time of the output signals. If T_r is the time taken by the response to change from 10% to 90% of its final value, the sensor's bandwidth is commonly calculated as $0.35/T_r$. This experiment was performed in two different scenarios, each of which repeated five times. At first, the sensor array without its silicone cover was tested where a bandwidth of 10 Hz, averaged among repetitions, was obtained. Next, the experiment was repeated for the encapsulated sensor array. In this scenario, the sensors showed a slower dynamic response with a bandwidth of approximately 1.49 Hz on average with the standard deviation of 0.705 Hz. This reduction in bandwidth is due to the sluggish, soft nature of the silicone membrane. Fig. 19 shows the bandwidth calculated for each individual sensor in the encapsulated array.

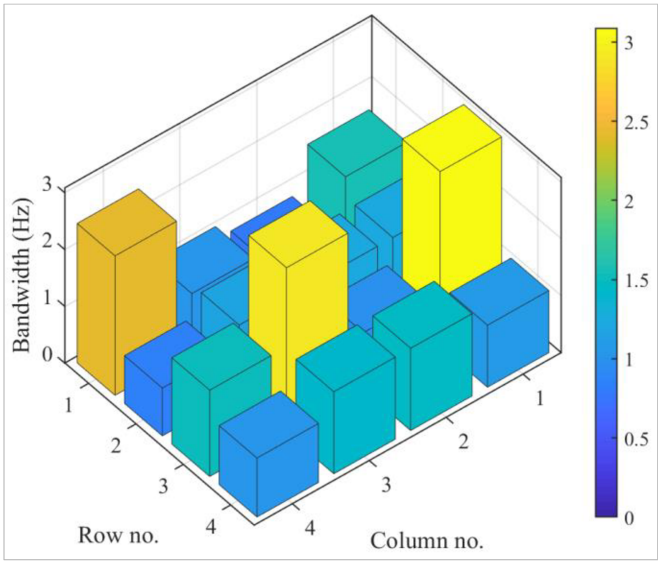

Fig. 19. Bandwidth of individual sensors in the encapsulated array

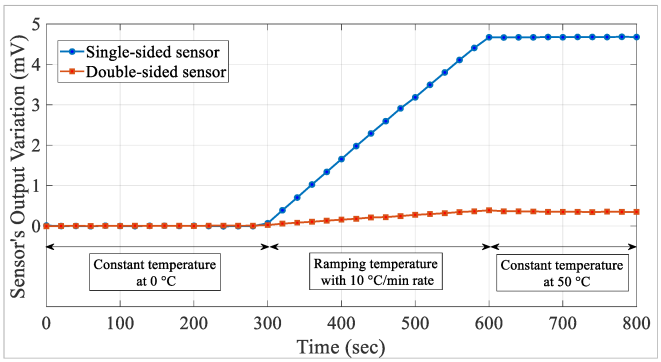

Fig. 20. Output signals collected from regular and temperature-compensated sensors in response to drastic temperature variation.

D. *Temperature sensitivity*

To experimentally validate the proposed thermal compensation technique, both single-sided and double-sided sensors were thermally stimulated inside a temperature-regulated chamber alongside each other. In this experiment, the sensors were directly pasted on the surface of the temperature-controlled plate inside the chamber while the temperature was dynamically changed within the range of 0-50 °C. In this experiment, the temperature was first kept constant at 0 °C for 5 minutes to allow the sensors to reach a thermal steady state, and then the temperature was increased to 50 °C with a constant rate of 10 °C/min. Fig. 20 shows a typical response collected from single- and double-sided sensors. According to the results,

the double-sided sensors show a temperature sensitivity of 6 nV/°C which is a 10-fold reduction to temperature stimulations as compared to single-sided sensors. Although there is still a drift in the double-sided sensors' output, which is due to slight dissimilarity between the paired gauges, this sensitivity can be further damped by the usage of sensors with matched temperature sensitivity.

The experimental results confirmed the effectiveness of the thermal compensation technique, which utilized a paired-sensor setting with a differential arrangement, enabling simultaneous enhancement in thermal compensation (i.e., 10 fold) and strain sensitivity (i.e., 2 fold). These enhancements are in par with, or better than, previously-reported studies in the literature similar to the configuration and methodology utilized in the present paper. For example, Lee and colleagues [58] used a temperature sensor and a micro-heater to keep temperature of their proposed piezoresistor at a constant value. As a result, they achieved approximately 4-fold attenuation in temperature drifts, although the measurement sensitivity was also reduced by 28% as compared to the configuration without thermal compensation (i.e., temperature control). Aryafar and colleagues [59] proposed a novel passive technique for thermal compensation of a piezoresistive pressure sensor, which achieved temperature insensitivity via the usage of resistors with negative temperature coefficient built in the sensor. Similarly, Engel and colleagues [60] fabricated metal strain gauges, which covered an extended length of underlying beams, leading to a 36% sensitivity enhancement in terms of gauge factor and strain measurement. Mohammad and colleagues [61] proposed piezoresistive stain sensors with enhanced strain sensitivity by introduction of geometric features in the sensor's carrier (e.g., slots and trenches). Similarly, Zhang [62] proposed metal strain gauges embedded in a flexible silicone matrix, and demonstrated 80% strain sensitivity enhancement by introduction of surface epidermal ridges on the membrane. For a comprehensive review of the literature on sensitivity enhancement and thermal compensation techniques refer to [63].

VI. Conclusion

In this study, we addressed issues regarding scalability of tactile skins in the context where the ultimate goal is to cover large-area robot surfaces. Specifically, a flexible robot skin was fabricated which consisted of an array of piezoresistive polymeric strain gauges micro-patterned on a flexible polyimide, and encased inside a compliant encapsulant. The strain gauges featured a biaxial symmetric response, avoiding insensitive regions in their vicinity thanks to their novel star-shaped geometry. The proposed gauge structure was first modeled in COMSOL® Multiphysics software in order to investigate a variety of geometry specifications under various stress-strain profiles and different loading locations with respect to the gauge's location. The finite-element simulations suggested that longer spokes and smaller spacing tend to achieve larger sensitivities on average.

Following simulation, gauges with the optimal structure parameters along with the interconnection terminals were printed onto a polyimide film using photolithographic processes. Subsequently, PEDOT:PSS, a piezoresistive polymer, was lithographically-patterned on top of the strain gauges via spin-coating and wet loft-off. In this investigation, a novel thermal compensation technique was proposed by homogeneous integration of strain gauges on the opposite sides of a flexible carrier. The temperature-compensated sensor not only gained a 10-fold attenuation in temperature sensitivity, but also featured a double sensitivity in terms of strain measurement. Upon lamination, in order to provide mechanical compliance and robustness against collision, a multi-step casting process was utilized to mold silicone polymer all around the sensor array.

A custom-made data acquisition system was developed based on precision electronic components and interfaced with the fabricated tactile array for signal conditioning and digitalization as well as transmission of data. For empirical validation of the developed robot skin, an automated testbed was implemented which was capable of scanning the array, applying controlled load on desired locations on the robot skin's surface, and collection of time-sensitive characterization data. The robot skin's behavior was investigated in terms of characteristic curve, hysteresis, spatial sensitivity, temperature sensitivity, and bandwidth. Furthermore, the empirical data were found to be in close agreement with the simulation trends obtained from FEA modeling in terms of biaxial sensitivity and circular symmetry. The FEA model enables future parametric studies of sensor structure, material properties, and package dimension in order to guide future design choices. In future work, comprehensive cyclic stability and fatigue tests, as well as analytical and empirical analysis of effect of layer thickness on the sensor's performance will be performed. Furthermore, the robot skin samples developed in this study will be used in future human-robot interaction and healthcare applications.

Acknowledgment

This work was supported by National Science Foundation grants #IIS-1208623, #IIP- 1534124, and #IIP-1713741. The authors wish to thank University of Louisville's Micro/Nano Technology Center for access to their facility. We also wish to thank Ruoshi Zhang, Sumit Das, and Brandon Young for their help with the experiments reported in this paper.

References

[1] C. Bartolozzi, L. Natale, F. Nori, and G. Metta, "Robots with a sense of touch," *Nature materials,* vol. 15, no. 9, p. 921, 2016.

[2] M. Johnsson and C. Balkenius, "Sense of touch in robots with self-organizing maps," *IEEE Transactions on Robotics,* vol. 27, no. 3, pp. 498-507, 2011.

[3] B. Ward-Cherrier, L. Cramphorn, and N. F. Lepora, "Tactile manipulation with a TacThumb integrated on the open-hand M2 gripper," *IEEE Robotics and Automation Letters,* vol. 1, no. 1, pp. 169-175, 2016.

[4] W. Kim, M. Lorenzini, K. Kapıcıoğlu, and A. Ajoudani, "ErgoTac: A Tactile Feedback Interface for Improving Human Ergonomics in Workplaces," *IEEE Robotics and Automation Letters,* vol. 3, no. 4, pp. 4179-4186, 2018.

[5] T. Mukai, M. Onishi, T. Odashima, S. Hirano, and Z. Luo, "Development of the tactile sensor system of a human-interactive robot "RI-MAN"," *IEEE Transactions on Robotics,* vol. 24, no. 2, pp. 505-512, 2008.

[6] S. Decherchi, P. Gastaldo, R. S. Dahiya, M. Valle, and R. Zunino, "Tactile-data classification of contact materials using computational intelligence," *IEEE Transactions on Robotics,* vol. 27, no. 3, pp. 635-639, 2011.

[7] H. Kristanto, P. Sathe, A. Schmitz, T. P. Tomo, S. Somlor, and S. Sugano, "A Wearable Three-Axis Tactile Sensor for Human Fingertips," *IEEE Robotics and Automation Letters,* vol. 3, no. 4, pp. 4313-4320, 2018.

[8] B. D. Argall and A. G. Billard, "A survey of tactile human–robot interactions," *Robotics and autonomous systems,* vol. 58, no. 10, pp. 1159-1176, 2010.

[9] S. Russo, R. Assaf, N. Carbonaro, and A. Tognetti, "Touch Position Detection in Electrical Tomography Tactile Sensors Through Quadratic Classifier," *IEEE Sensors Journal,* 2018.

[10] M. N. Saadatzi, S. K. Das, I. B. Wijayasinghe, D. O. Popa, and J. R. Baptist, "Precision Grasp Control with a Pneumatic Gripper and a Novel Fingertip Force Sensor," in *2018 IEEE 14th International Conference on Automation Science and Engineering (CASE)*, 2018, pp. 1454-1459.

[11] G. Herrmann and C. Melhuish, "Towards safety in human robot interaction," *International Journal of Social Robotics,* vol. 2, no. 3, pp. 217-219, 2010.

[12] R. S. Dahiya, P. Mittendorfer, M. Valle, G. Cheng, and V. J. Lumelsky, "Directions toward effective utilization of tactile skin: A review," *IEEE Sensors Journal,* vol. 13, no. 11, pp. 4121-4138, 2013.

[13] S. Stassi, V. Cauda, G. Canavese, and C. F. Pirri, "Flexible tactile sensing based on piezoresistive composites: A review," *Sensors,* vol. 14, no. 3, pp. 5296-5332, 2014.

[14] X. Wang, L. Dong, H. Zhang, R. Yu, C. Pan, and Z. L. Wang, "Recent progress in electronic skin," *Advanced Science,* vol. 2, no. 10, p. 1500169, 2015.

[15] V. J. Lumelsky, M. S. Shur, and S. Wagner, "Sensitive skin," *IEEE Sensors Journal,* vol. 1, no. 1, pp. 41-51, 2001.

[16] P. Mittendorfer and G. Cheng, "Humanoid multimodal tactile-sensing modules," *IEEE Transactions on robotics,* vol. 27, no. 3, pp. 401-410, 2011.

[17] A. Schmitz, P. Maiolino, M. Maggiali, L. Natale, G. Cannata, and G. Metta, "Methods and technologies for the implementation of large-scale robot tactile sensors," *IEEE Transactions on Robotics,* vol. 27, no. 3, pp. 389-400, 2011.

[18] N. F. Lepora, U. Martinez-Hernandez, M. Evans, L. Natale, G. Metta, and T. J. Prescott, "Embodied hyperacuity for robot touch," in *Proceedings of the IEEE International Conference on Robotics and Automation (ICRA)*, 2013.

[19] T. Mukai, S. Hirano, and Y. Kato, "Fast and accurate tactile sensor system for a human-interactive robot," in *Sensors: Focus on Tactile Force and Stress Sensors*: InTech, 2008.

[20] T. Asfour, K. Regenstein, P. Azad, J. Schroder, A. Bierbaum, N. Vahrenkamp, and R. Dillmann, "ARMAR-III: An integrated humanoid platform for sensory-motor control," in *2006 6th IEEE-RAS international conference on humanoid robots*, 2006, pp. 169-175.

[21] H. Iwata and S. Sugano, "Design of human symbiotic robot TWENDY-ONE," in *2009 IEEE International Conference on Robotics and Automation*, 2009, pp. 580-586.

[22] G. Cannata, M. Maggiali, G. Metta, and G. Sandini, "An embedded artificial skin for humanoid robots," in *2008 IEEE International Conference on Multisensor Fusion and Integration for Intelligent Systems*, 2008, pp. 434-438.

[23] E. Cheung and V. J. Lumelsky, "Proximity sensing in robot manipulator motion planning: system and implementation issues," *IEEE transactions on Robotics and Automation,* vol. 5, no. 6, pp. 740-751, 1989.

[24] T. Someya, Y. Kato, T. Sekitani, S. Iba, Y. Noguchi, Y. Murase, H. Kawaguchi, and T. Sakurai, "Conformable, flexible, large-area networks of pressure and thermal sensors with organic transistor active matrixes," *Proceedings of the National Academy of Sciences,* vol. 102, no. 35, pp. 12321-12325, 2005.

[25] Y. Ohmura, Y. Kuniyoshi, and A. Nagakubo, "Conformable and scalable tactile sensor skin for curved surfaces," in *Proceedings 2006 IEEE International Conference on Robotics and Automation, 2006. ICRA 2006.*, 2006, pp. 1348-1353: IEEE.

[26] T. P. Tomo, M. Regoli, A. Schmitz, L. Natale, and H. Kristanto, "A New Silicone Structure for uSkin—A Soft, Distributed, Digital 3-Axis Skin Sensor and Its Integration on the Humanoid Robot iCub," *IEEE Robotics and Automation Letters,* vol. 3, no. 3, pp. 2584-2591, 2018.

[27] M. N. Saadatzi, C. K. Robinson, and D. O. Popa, "Advanced Tactile Perception for Materials Handling and Collaborative Robotics in Industrial Tasks," National Institute of Standards and Technology (NIST) Workshop on Robotic Assembly – Recent Advancements and Opportunities for Challenging R&D.

[28] M. L. Hammock, A. Chortos, B. C. K. Tee, J. B. H. Tok, and Z. Bao, "25th anniversary article: the evolution of electronic skin (e-skin): a brief history, design considerations, and recent progress," *Advanced materials,* vol. 25, no. 42, pp. 5997-6038, 2013.

[29] N. Lu and D.-H. Kim, "Flexible and stretchable electronics paving the way for soft robotics," *Soft Robotics,* vol. 1, no. 1, pp. 53-62, 2014.

[30] S. Stassi, V. Cauda, G. Canavese, and C. Pirri, "Flexible tactile sensing based on piezoresistive composites: A review," *Sensors,* vol. 14, no. 3, pp. 5296-5332, 2014.

[31] N. Yogeswaran *et al.*, "New materials and advances in making electronic skin for interactive robots," *Advanced Robotics,* vol. 29, no. 21, pp. 1359-1373, 2015.

[32] M. Eltaib and J. Hewit, "Tactile sensing technology for minimal access surgery—a review," *Mechatronics,* vol. 13, no. 10, pp. 1163-1177, 2003.

[33] H. Takao, M. Yawata, K. Sawada, and M. Ishida, "A multifunctional integrated silicon tactile imager with arrays of strain and temperature sensors on single crystal silicon diaphragm," *Sensors and Actuators A: Physical,* vol. 160, no. 1-2, pp. 69-77, 2010.

[34] H. Takao, K. Sawada, and M. Ishida, "Multifunctional smart tactile-image sensor with integrated arrays of strain and temperature sensors on single air-pressurized silicon diaphragm," in *Solid-State Sensors, Actuators and Microsystems, 2005. Digest of Technical Papers. TRANSDUCERS'05. The 13th International Conference on*, 2005, vol. 1, pp. 45-48.

[35] H. Takao, K. Sawada, and M. Ishida, "Silicon smart tactile image sensor with pneumatically swollen single diaphragm structure," in *Micro Electro Mechanical Systems, 2004. 17th IEEE International Conference on.(MEMS)*, 2004, pp. 846-849.

[36] H. Wang *et al.*, "Tuning the threshold voltage of carbon nanotube transistors by n-type molecular doping for robust and flexible complementary circuits," *Proceedings of the National Academy of Sciences,* p. 201320045, 2014.

[37] W. Wu, X. Wen, and Z. L. Wang, "Taxel-addressable matrix of vertical-nanowire piezotronic transistors for active/adaptive tactile imaging," *Science,* p. 1234855, 2013.

[38] S. M. Won *et al.*, "Piezoresistive strain sensors and multiplexed arrays using assemblies of single-crystalline silicon nanoribbons on plastic substrates," *IEEE Transactions on Electron Devices,* vol. 58, no. 11, pp. 4074-4078, 2011.

[39] C. S. Smith, "Piezoresistance effect in germanium and silicon," *Physical review,* vol. 94, no. 1, p. 42, 1954.

[40] K. Kim *et al.*, "Polymer-based flexible tactile sensor up to 32× 32 arrays integrated with interconnection terminals," *Sensors and Actuators A: Physical,* vol. 156, no. 2, pp. 284-291, 2009.

[41] W.-C. Choi, "Polymer micromachined flexible tactile sensor for three-axial loads detection," *Transactions on electrical and electronic materials,* vol. 11, no. 3, pp. 130-133, 2010.

[42] J. Engel, J. Chen, Z. Fan, and C. Liu, "Polymer micromachined multimodal tactile sensors," *Sensors and Actuators A: physical,* vol. 117, no. 1, pp. 50-61, 2005.

[43] Y.-J. Yang *et al.*, "An integrated flexible temperature and tactile sensing array using PI-copper films," *Sensors and Actuators A: Physical,* vol. 143, no. 1, pp. 143-153, 2008.

[44] I. Graz *et al.*, "Flexible active-matrix cells with selectively poled bifunctional polymer-ceramic nanocomposite for pressure and temperature sensing skin," *Journal of Applied Physics,* vol. 106, no. 3, p. 034503, 2009.

[45] G. Witt, "The electromechanical properties of thin films and the thin film strain gauge," *Thin Solid Films,* vol. 22, no. 2, pp. 133-156, 1974.

[46] F. A. Vreede and N. M. E. R. I. G. Division, *Measuring Plane States of Stress with Regular Strain Gauge Rosettes*. CSIR, 1981.

[47] G. Y. Yang, V. J. Bailey, G. Lin, W. C. Tang, and J. H. Keyak, "Design of microfabricated strain gauge array to monitor bone deformation in vitro and in vivo," in *Bioinformatics and Bioengineering, 2004. BIBE 2004. Proceedings. Fourth IEEE Symposium on*, 2004, pp. 30-37: IEEE.

[48] G. Latessa, F. Brunetti, A. Reale, G. Saggio, and A. Di Carlo, "Piezoresistive behaviour of flexible PEDOT: PSS based sensors," *Sensors and Actuators B: Chemical,* vol. 139, no. 2, pp. 304-309, 2009.

[49] H. Al-Chami, "Inkjet printing of transducers," University of British Columbia, 2010.

[50] J. R. Castrejon-Pita, W. Baxter, J. Morgan, S. Temple, G. Martin, and I. Hutchings, "Future, opportunities and challenges of inkjet technologies," *Atomization and sprays,* vol. 23, no. 6, 2013.

[51] Z. Yin, Y. Huang, N. Bu, X. Wang, and Y. Xiong, "Inkjet printing for flexible electronics: Materials, processes and equipments," *Chinese Science Bulletin,* vol. 55, no. 30, pp. 3383-3407, 2010.
[52] S. Kommeren, M. J. Coenen, T. M. Eggenhuisen, T. W. Slaats, H. Gorter, and P. Groen, "Combining solvents and surfactants for inkjet printing PEDOT: PSS on P3HT/PCBM in organic solar cells," *Organic Electronics,* vol. 61, pp. 282-288, 2018.
[53] Z. Xiong and C. Liu, "Optimization of inkjet printed PEDOT: PSS thin films through annealing processes," *Organic Electronics,* vol. 13, no. 9, pp. 1532-1540, 2012.
[54] C. Srichan *et al.*, "Inkjet printing PEDOT: PSS using desktop inkjet printer," in *2009 6th International Conference on Electrical Engineering/Electronics, Computer, Telecommunications and Information Technology*, 2009, vol. 1, pp. 465-468.
[55] J. R. Baptist, R. Zhang, D. Wei, M. N. Saadatzi, and D. O. Popa, "Fabrication of strain gauge based sensors for tactile skins," in *Smart Biomedical and Physiological Sensor Technology XIV*, 2017, vol. 10216, p. 102160F: International Society for Optics and Photonics.
[56] M. N. Saadatzi, J. R. Baptist, I. B. Wijayasinghe, and D. O. Popa, "Characterization of large-area pressure sensitive robot skin," in *Smart Biomedical and Physiological Sensor Technology XIV*, 2017, vol. 10216, p. 102160G: International Society for Optics and Photonics.
[57] M. N. Saadatzi, Z. Yang, J. R. Baptist, R. R. Sahasrabuddhe, I. B. Wijayasinghe, and D. O. Popa, "Parametric investigation of scalable tactile sensors," in *Smart Biomedical and Physiological Sensor Technology XIV*, 2017, vol. 10216, p. 102160A: International Society for Optics and Photonics.
[58] K. Lee, H. Takao, K. Sawada, and M. Ishida, "Analysis of thermal drift of a constant temperature control type three-axis accelerometer for high temperatures," *IEEJ Transactions on Sensors and Micromachines,* vol. 123, no. 12, pp. 583-587, 2003.
[59] M. Aryafar, M. Hamedi, and M. Ganjeh, "A novel temperature compensated piezoresistive pressure sensor," *Measurement,* vol. 63, pp. 25-29, 2015.
[60] J. Engel, J. Chen, and C. Liu, "Strain sensitivity enhancement of thin metal film strain gauges on polymer microscale structures," *Applied physics letters,* vol. 89, no. 22, p. 221907, 2006.
[61] A. Mohammed, W. Moussa, and E. Lou, "High sensitivity MEMS strain sensor: design and simulation," *Sensors,* vol. 8, no. 4, pp. 2642-2661, 2008.
[62] Y. Zhang, "Sensitivity enhancement of a micro-scale biomimetic tactile sensor with epidermal ridges," *Journal of micromechanics and microengineering,* vol. 20, no. 8, p. 085012, 2010.
[63] A. Fiorillo, C. Critello, and A. Pullano, "Theory, technology and applications of piezoresistive sensors: A review," *Sensors and Actuators A: Physical,* 2018.

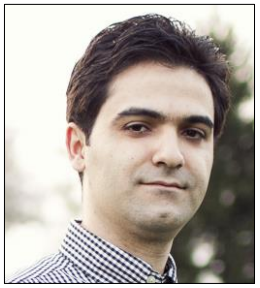

Mohammad N. Saadatzi was born in Iran, in 1982, where he studied Electrical Engineering and received his B.Sc. and M.Sc in 2004 and 2010, respectively. He then moved to the United States and received a Ph.D. degree in Electrical and Computer Engineering from the University of Louisville, KY in 2016. He then joined the Next Generation Systems (NGS) Group at the University of Louisville as a Postdoctoral Research Associate. His current research interests are advanced human-machine interfaces, assistive robotics, instrumentation, and affective computing.

Joshua R. Baptist is a Research and Development Specialist with the Next Generation Systems (NGS) group at the University of Louisville in Louisville, Kentucky. He joined the NGS group in 2014 with prior experience in solid-state physics and mechanical design. He maintains multi-disciplinary interests in science and engineering whose disciplines supported many technical research endeavors at the NGS Group. His interests include Mechanics, Atomics, Electricity, and Magnetism.

Zhong Yang is a Ph.D. candidate with the Next Generation Systems (NGS) Research Group at University of Louisville, Louisville, KY. He received his B.Sc. in electrical and electronics engineering from the Tianjin University, China, in 2012, and his M.Sc. from University of Arizona in 2016. He joined the NGS research Group in 2016 as a graduate research assistant with a background in software development, modeling and control, and MEMS design. His current research interests include microrobots and reduce-order modeling.

Dan O. Popa (SM ’16, M’93) received a BA in Engineering, Mathematics and Computer Science and a MS in Engineering, both from Dartmouth College, USA, in 1993 and 1994, respectively. He received a PhD in EE from Rensselaer Polytechnic Institute (RPI) in 1998, focusing on motion planning for nonholonomic robots. In 1998 he joined the Center for Automation Technologies at RPI, where he held the rank of Senior Research Scientist. In 2004, he became Assistant and then Associate Professor of Electrical Engineering at the University of Texas at Arlington, USA until 2015. Since 2016, he is the Vogt Endowed Chair in Advanced Manufacturing, and Professor of Electrical and Computer Engineering at the University of Louisville. He is currently head of the Next Generation Research Group (NGS) conducting research in two main areas: 1) the design, characterization, modeling and control of microactuators and precision robots, and 2) social and physical human-robot interaction through adaptive interfaces and robot skin. Prof. Popa is the recipient of several prestigious awards and the author of over 150 refereed conference and journal papers, book chapters published in IEEE and ASME societies.